Experimental Validation of Low-Z Ion-Stopping Formalisms around the Bragg Peak in High-Energy-Density Plasmas

J. A. Frenje,[1] R. Florido,[2] R. Mancini,[3] T. Nagayama,[4] P. E. Grabowski,[5] H. Rinderknecht,[7] H. Sio,[1] A. Zylstra,[6] M. Gatu Johnson,[1] C. K. Li,[1] F. H. Séguin,[1] R. D. Petrasso,[1] V. Yu Glebov,[7] and S. P. Regan[7]

[1]*Plasma Science and Fusion Center, Massachusetts Institute of Technology, Cambridge, Massachusetts 02139, USA*
[2]*iUNAT–Departamento de Física, Universidad de Las Palmas de Gran Canaria, 35017 Las Palmas de Gran Canaria, Spain*
[3]*Physics Department, University of Nevada, Reno, Nevada 89557, USA*
[4]*Sandia National Laboratory, Albuquerque, New Mexico 87185, USA*
[5]*Lawrence Livermore National Laboratory, Livermore, California 94550, USA*
[6]*Los Alamos National Laboratory, Los Alamos, New Mexico 87545, USA*
[7]*Laboratory for Laser Energetics, University of Rochester, Rochester, New York 14623, USA*

(Received 5 August 2018; revised manuscript received 21 October 2018; published 8 January 2019)

We report on the first accurate validation of low-Z ion-stopping formalisms in the regime ranging from low-velocity ion stopping—through the Bragg peak—to high-velocity ion stopping in well-characterized high-energy-density plasmas. These measurements were executed at electron temperatures and number densities in the range of 1.4–2.8 keV and 4×10^{23}–8×10^{23} cm^{-3}, respectively. For these conditions, it is experimentally demonstrated that the Brown-Preston-Singleton formalism provides a better description of the ion stopping than other formalisms around the Bragg peak, except for the ion stopping at $v_i \sim 0.3 v_{\text{th}}$, where the Brown-Preston-Singleton formalism significantly underpredicts the observation. It is postulated that the inclusion of nuclear-elastic scattering, and possibly coupled modes of the plasma ions, in the modeling of the ion-ion interaction may explain the discrepancy of ~20% at this velocity, which would have an impact on our understanding of the alpha energy deposition and heating of the fuel ions, and thus reduce the ignition threshold in an ignition experiment.

DOI: 10.1103/PhysRevLett.122.015002

In hot-spot ignition experiments [1] at the National Ignition Facility [2], which use deuterium-tritium (DT) fuel, an understanding of the DT-alpha energy deposition and heating of the high-energy-density (HED) plasma is critical for determining the ignition threshold. This requires a fundamental understanding of the DT-alpha stopping around the Bragg peak, where the ion velocity (v_i) is similar to the average velocity (v_{th}) of the thermal plasma electrons, for a wide range of electron (T_e) and ion temperatures (T_i), and electron-number densities (n_e) [3]. Ion stopping in HED plasmas has therefore been subject to extensive analytical and numerical studies for decades [4–14], but a theoretical treatment of ion stopping, especially around the Bragg peak, remains a difficult problem. The consensus is that the ion stopping at $v_i \gg v_{\text{th}}$ is treated well by the Born approximation [12] because the interaction between the fast ions and the plasma electrons is small, resulting in small energy transfers compared to the kinetic energy of the ions. At $v_i < v_{\text{th}}$, the ion stopping is harder to characterize but generally described by collisional theories that treat two-body collisions and large-angle scattering between the ions and the plasma electrons [13,15]. At ion velocities near v_{th}, the Born approximation breaks down because scattering is no longer weak and collisional theories have difficulty providing a complete, self-consistent picture of the ion stopping due to the dynamic dielectric response of the plasma electrons. Rigorous quantum mechanical treatments based on convergent kinetic theories [6,14,16] try to rectify these challenges by utilizing the strengths of the different approaches applied to the different regimes; however, it is not clear how best to combine them and quantify their errors. Precise measurements of the ion stopping around the Bragg peak are therefore essential to guiding the theoretical efforts.

Although numerous efforts have been made to theoretically describe the behavior of ion stopping in HED plasmas, only a limited set of experimental data exists to test these theories. In addition, most of these experiments used only one particle with a distinct velocity in the high-velocity ion-stopping regime ($v_i > v_{\text{th}}$) [17–30] and thus did not simultaneously probe the detailed characteristics of the Bragg peak below and above v_{th}. To the best of our knowledge, only two experiments have made an attempt to simultaneously probe the low- and high-velocity sides of the Bragg peak. The first experiment was conducted by Hicks *et al.* [28], who provided a qualitative description of the ion stopping around the Bragg peak. The second one was conducted by Frenje *et al.* [29], who provided the first experimental evidence that the position and magnitude of

TABLE I. Experimental parameters and key HED-plasma parameters.

Shot	Capsule[a]	Laser	Bang times [ps][b]			T_i[c]	DD	D^3He	$T_{e,0}$[d]	$\langle T_e\rangle$[e]	$\langle n_e\rangle$[f]	$\langle n_eL\rangle$[g]
		[kJ]	D^3He	DD	X ray	(keV)	Yield	Yield	(keV)	(keV)	$[\times10^{23}\,cm^{-3}]$	$[\times10^{21}\,cm^{-2}]$
75694	$^3He(6.8)D_2(3)Ar(0.15)SiO_2$[2.7]	12.0	1065	1100	1140	8.8 ± 0.3	1.5×10^{10}	1.1×10^{10}	4.4 ± 0.4	2.8 ± 0.3	6.6 ± 1.0	4.1 ± 0.4
75703	$^3He(7.1)D_2(3)Ar(0.14)SiO_2$[2.8]	11.7	1085	1142	1180	8.3 ± 0.3	1.4×10^{10}	7.4×10^{9}	4.2 ± 0.4	2.5 ± 0.3	8.2 ± 1.0	4.2 ± 0.4
75695	$^3He(6.7)D_2(3)Ar(0.14)SiO_2$[2.7]	9.9	1095	1163	1215	7.8 ± 0.3	1.1×10^{10}	5.9×10^{9}	4.1 ± 0.4	2.3 ± 0.2	4.6 ± 0.7	4.5 ± 0.5
75698	$^3He(6.0)D_2(3)Ar(0.14)SiO_2$[2.7]	9.9	1110	1173	1220	7.6 ± 0.3	1.1×10^{10}	5.3×10^{9}	4.0 ± 0.4	2.1 ± 0.2	4.8 ± 0.7	4.3 ± 0.4
75699	$^3He(6.7)D_2(3)Ar(0.14)SiO_2$[2.7]	8.1	1195	1254	1290	6.6 ± 0.3	7.3×10^{9}	2.3×10^{9}	3.7 ± 0.4	1.9 ± 0.2	3.9 ± 0.6	3.9 ± 0.4
75700	$^3He(6.7)D_2(3)Ar(0.12)SiO_2$[2.7]	8.0	1185	1258	1300	7.0 ± 0.3	6.6×10^{9}	2.1×10^{9}	3.6 ± 0.4	1.9 ± 0.2	3.8 ± 0.6	4.2 ± 0.4
75701	$^3He(6.7)D_2(3)Ar(0.12)SiO_2$[2.6]	6.6	1330	1360	1430	4.6 ± 0.3	2.7×10^{9}	3.2×10^{8}	3.1 ± 0.3	1.8 ± 0.2	5.1 ± 0.8	3.2 ± 0.3
75702	$^3He(6.5)D_2(3)Ar(0.15)SiO_2$[2.8]	6.3	1350	1398	1525	4.5 ± 0.3	2.4×10^{9}	2.7×10^{8}	3.0 ± 0.3	1.4 ± 0.1	3.8 ± 0.6	5.2 ± 0.5

[a] ^{3}He, D_2, and Ar gas pressures (in atm), and SiO_2 capsule thicknesses (in μm). The capsule diameter is on average ~920 μm.
[b] Measured x-ray, DD, and D^3He bang times using the Particle X-ray Temporal Diagnostic [33].
[c] DD-burn-averaged, apparent burn-averaged ion temperature $\langle T_i\rangle$ determined from the measured NTOF signal [34], and DD-D^3He yield ratio.
[d] $T_{e,0}$ inferred from the measured x-ray spectrum in the range of 20–80 keV using the Hard X-ray Detector [35]. This value is strongly weighted towards the center of the implosion.
[e,f] $\frac{dE}{dx}$-weighted $\langle T_e\rangle$ and $\langle n_e\rangle$ determined from the measured $n_e(r,t)$ and $T_e(r,t)$ profiles at DD bang time using the Multiple Monochromatic Imager (MMI) [32]. These plasma conditions correspond to an electron and ion plasma-coupling parameter in ranges of 0.007–0.012 and 0.005–0.010, respectively, which indicate weakly coupled HED plasmas. As dE/dx scales with n_e/T_e, these values represent the colder and denser plasma surrounding the hotter core.
[g] Path-length-integrated $\langle n_eL\rangle$, where $\langle L\rangle$ is the average path length of the fusion products through the spherical HED plasma. The uncertainties are weighted averages of measurements and modeling.

the Bragg peak depends strongly on T_e. However, the limitation of both of these experiments was that the HED-plasma conditions could not be diagnosed to the level required for experimental validation of various ion-stopping formalisms. The work described in this Letter significantly advances previous efforts by providing the first accurate experimental validation of ion-stopping formalisms in the regime ranging from low-velocity ion stopping—through the Bragg peak—to high-velocity ion stopping in well-characterized HED-plasma conditions.

The experiments reported herein were carried out at OMEGA [31], where eight deuterium-helium-3 gas-filled capsules were symmetrically imploded with 60 laser beams, delivering up to 12.0 kJ to the capsule in a 1-ns square pulse. As shown in Table I, each SiO_2 capsule had a shell thickness of ~2.7 μm and an initial D^3He-gas-fill pressure in the range of 12 to 13 atm. These capsules were also filled with a small amount of argon for a time- and space-resolved measurement of the electron-temperature and electron-number-density profiles [32].

Essential to this Letter is to accurately characterize the spatially and temporally varying HED-plasma conditions during the nuclear-production period. For this, an unprecedented set of complementary nuclear and x-ray measurements was conducted, as illustrated in Table I and Figs. 1 and 2. Table I shows measured nuclear and x-ray bang times, burn-averaged T_i, DD and D^3He yields, and T_e at the center of the implosion for all shots. Implosion parameters inferred from the measured data, essential to the ion-stopping predictions, are also shown in Table I. It is also notable that each shot pair at a given laser energy is producing reproducible data. Figure 1 shows the measured and modeled x-ray-emission history, and the DD-burn and D^3He-burn histories together with the implosion trajectory for shot 75699, while Fig. 2 shows measured electron-number-density and electron-temperature profiles

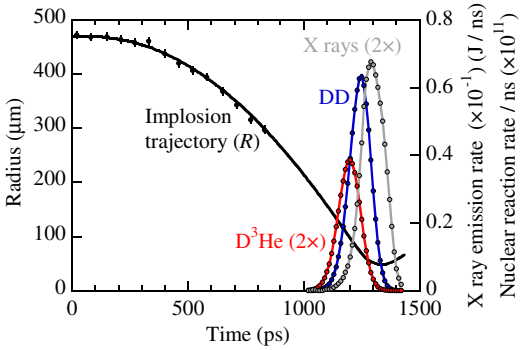

FIG. 1. Measured (points) and modeled (solid curves) nuclear-burn and x-ray-emission histories, and implosion trajectory for shot 75699. The x-ray-emission history was determined from x rays measured in the energy range of 3.375–3.600 keV. The implosion trajectory, which is well modeled by a 1D HYADES simulation, was measured with a time-gated imaging camera probing soft x rays from the SiO_2 shell.

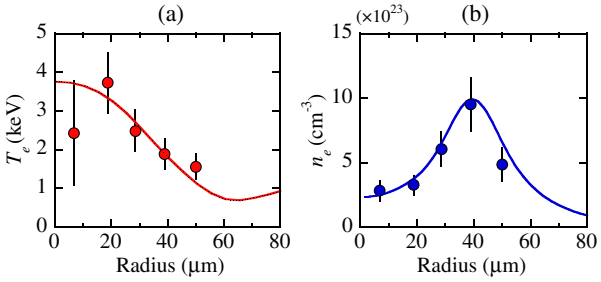

FIG. 2. Profiles of (a) electron-temperature and (b) electron-number density for shot 75699 electron-temperature and electron-number density for shot 75699, measured by the MMI (data points) and simulated by HYADES (solid curves). These profiles were integrated over a time window of 1.23–1.33 ns and are x-ray emissivity weighted towards the end of the time window. To match the measured profiles, scaling factors in the ranges of 1.2–1.6 and 0.7–0.9 were applied to the HYADES-simulated electron-temperature and electron-number-density profiles for the eight shots, respectively.

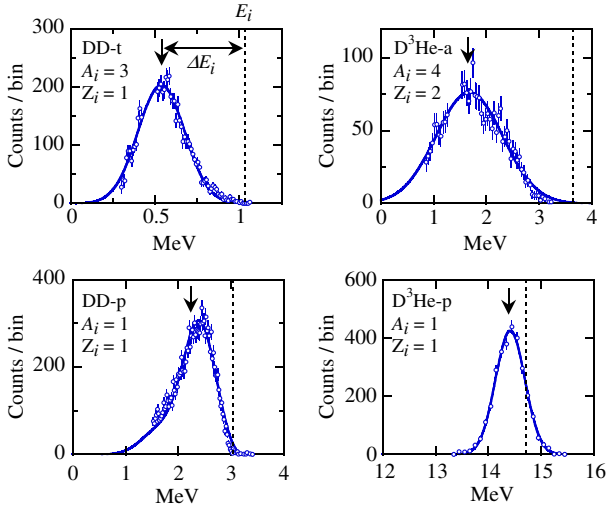

FIG. 3. Measured spectra of DD-t, D^{3}He-α, DD-p, and D^{3}He-p for shot 75699. These fusion products are produced by the reactions $\mathrm{D}+\mathrm{D}\rightarrow t(1.01\,\mathrm{MeV})+p(3.02\,\mathrm{MeV})$ and $\mathrm{D}+{}^3\mathrm{He}\rightarrow {}^4\mathrm{He}(3.71\,\mathrm{MeV})+p(14.63\,\mathrm{MeV})$, where the energies in the parentheses are the fusion-product birth energies (at zero ion temperature).

contrasted to HYADES simulations [36] for the same shot. From Table I and Fig. 2, it is clear that the 1D-simulated T_e profiles at the center of the implosion agree well with the measured $T_{e,0}$ value, which raises our confidence that the measured and inferred implosion parameters used for the ion-stopping predictions are determined with high accuracy (∼10% considering all measurements and modeling). As illustrated in Table I, it is also notable that the burn-averaged T_i values are significantly higher than the measured T_e. The reason for this is that the converging shock predominantly transfers energy to the heavier ions in the HED plasma. As the shock rebounds at the center of the implosion, it significantly raises T_i and n_i and initiates the DD and D^{3}He nuclear reactions. Given that the ion-ion equilibration time is ∼50 ps for these HED-plasma conditions, the ions are not fully in thermal equilibrium at the end of the ∼170 ps long burn, and as a consequence the neutron-time-of-flight (NTOF)-measured values in Table I represent an apparent T_i. In addition, as the ions and electrons do not have time to fully equilibrate during burn (the ion-electron thermalization time is ∼500 ps), the measured T_e is consequently lower than the measured apparent T_i. By contrast, the electron-electron thermalization time is subpicosecond for these conditions, which implies that the electrons are internally in thermal equilibrium and are well described by the HYADES simulations. From a burn-averaged point of view, assigning T_e to these plasmas is therefore meaningful.

For accurate experimental validation of the ion stopping around the Bragg peak, the energy losses ($-\Delta E_i$) of DD tritons (DD-t), DD protons (DD-p), D^{3}He alphas (D^{3}He-α) and D^{3}He protons (D^{3}He-p), while traversing the well-characterized HED-plasma conditions, were simultaneously measured. An example of measured spectra of DD-t, DD-p, D^{3}He-α, and D^{3}He-p is shown in Fig. 3 for shot 75699 (see the detailed discussion about these measurements and the associated uncertainties in the Supplemental Material [37]). These spectra were measured with a single spectrometer, but other spectrometers fielded around the implosion were also used for these measurements [38]. The vertical arrows in Fig. 3 indicate the median energy for each measured spectrum, and by contrasting these energies to the average-birth energies (vertical dashed lines), $-\Delta E_i$ was determined to an accuracy of ∼10% (see the Supplemental Material [37]) and used for the assessment of the ion stopping in the HED plasma. As the fusion products traverse the HED plasma with varying electron temperatures and electron-number densities (see Fig. 2), they probe different dE/dx-weighted $\langle T_e\rangle$ and $\langle n_e\rangle$ that need to be considered in the analysis of the data. Using a 3D Monte Carlo transport code and measured DD and D^{3}He source profiles using the proton core imaging system [39], it was determined that the low-velocity fusion products (DD-t, D^{3}He-α, and DD-p) probed a dE/dx-weighted $\langle T_e\rangle$ of 1.5 to 1.6 keV for shot 75699, while the D^{3}He-p probed a dE/dx-weighted $\langle T_e\rangle$ of 1.9 keV. This difference is smaller for the higher-$\langle T_e\rangle$ shots. In Table I, the D^{3}He-p dE/dx-weighted $\langle T_e\rangle$ and $\langle n_e\rangle$ values are shown.

To illustrate the measured energy loss of fusion products with different initial energy (E_i), charge (Z_i), and mass (A_i) passing through a HED plasma, the energy-loss data must be presented in the form of $-\Delta E_i/Z_i^2$ versus E_i/A_i. Figure 4 shows $-\Delta E_i/Z_i^2$ versus E_i/A_i for all shots, where the measured $-\Delta E_i$ values for the low-velocity fusion products were corrected for based on the different dE/dx-weighted $\langle T_e\rangle$ values, while the $-\Delta E_i$ value for the D^{3}He-p was corrected for the burn-averaged $\langle n_e L\rangle$ change from the

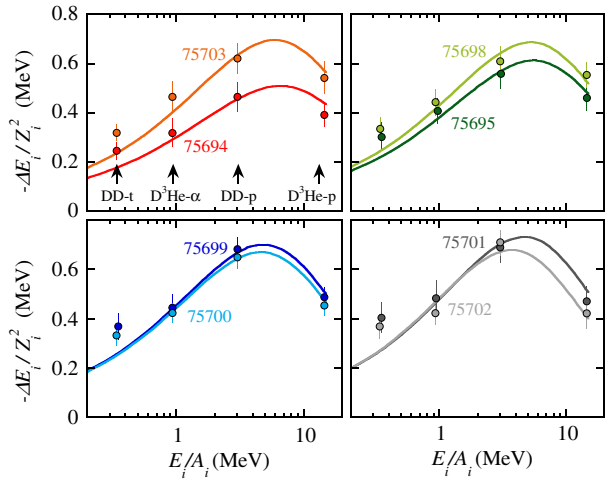

FIG. 4. Measured and predicted ion stopping ($-\Delta E_i/Z_i^2$) as a function of E_i/A_i for all shots. The data set is contrasted against BPS predictions (considering only ion-electron Coulomb interactions) for the measured $\langle T_e \rangle$ and $\langle n_e L \rangle$ values shown in Table I.

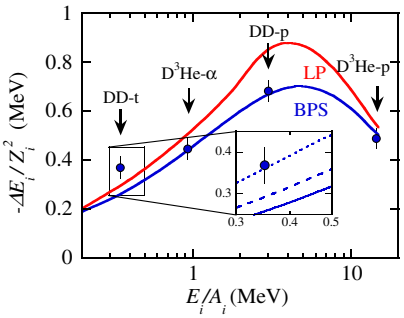

FIG. 5. Measured and predicted ion stopping ($-\Delta E_i/Z_i^2$) as a function of E_i/A_i for shot 75699. The blue and red curves represent the BPS and LP predictions, respectively, for the measured $\langle T_e \rangle$ and $\langle n_e L \rangle$ values shown in Table I. (Inset) The graph illustrates the DD-t data point, BPS predictions for tritons interacting only with electrons (solid blue), tritons interacting with electrons and ions (dashed blue), and tritons interacting with electrons and ions where the ion-ion component has been increased to enhance the total ion stopping by 20% (dotted blue).

D^3He-BT to DD-BT, as discussed in the Supplemental Material [37]. The solid curves in Fig. 4 were obtained by integrating the Brown-Preston-Singleton (BPS) plasma-stopping-power function, describing only the ion-electron Coulomb interaction, for the dE/dx-weighted $\langle T_e \rangle$ and $\langle n_e L \rangle$ values shown in Table I. Clearly, the data demonstrate that the BPS formalism is providing a good description of the ion stopping for these HED-plasma conditions, except for the stopping of DD-t at $v_i \sim 0.3 v_{\mathrm{th}}$. At this velocity, the BPS formalism systematically underpredicts DD-t energy loss for all shots. A systematic error in the measured DD-t energy loss can be ruled out in explaining this observation, as similar systematic errors would be evident in the measured D^3He-α and DD-p energy loss. An ion-bulk flow of ~500 km/s systematically in the direction away from the spectrometer, necessary to explain the observation, can also be excluded because spectrometers with nearly orthogonal lines of sight observe similar energy loss, and it would also be evident in the measured D^3He-α and DD-p spectra. A systematically too high DD-t dE/dx-weighted $\langle T_e \rangle$ for all shots can also be ruled out because a 300–400 eV lower value is required to explain the data, which is not plausible.

To examine the different ion-stopping formalisms routinely used in the field of inertial confinement fusion and to illustrate different approaches in unifying the different physical processes that dictate the characteristics of the Bragg peak, Fig. 5 contrasts the energy-loss data with predictions by BPS and Li and Petrasso (LP) [7] for shot 75699. As shown by the comparison, the BPS formalism is providing a better description of the Bragg peak, which supports the general view that the BPS formalism is considered to more accurately unify the binary-collision and dielectric-response formalisms with more rigorous quantum-diffraction corrections to the total ion stopping at $v_i \sim v_{\mathrm{th}}$. On the other hand, the BPS formalism, considering only ion-electron Coulomb interactions, systematically underpredicts the DD-t energy loss at $v_i \sim 0.3 v_{\mathrm{th}}$ for all shots. This observation cannot be explained by the inclusion of ion-ion Coulomb scattering in the modeling because ion-stopping theories based on multi-ion-component responses predict that the contribution of the ion-ion Coulomb scattering to the total DD-t plasma-stopping power is ~10% at $v_i \sim 0.3 v_{\mathrm{th}}$ [40] (see the dashed curve in the inset of Fig. 5). This points to the idea that the contribution from the ion-ion component to the total ion stopping at this velocity could in fact be larger than predicted by the theories. This is certainly plausible, as all theories ignore the ion-ion nuclear-elastic scattering, which is more strongly weighted towards large-angle scattering than Coulomb scattering. To explain the data at $v_i \sim 0.3 v_{\mathrm{th}}$, the total ion stopping must be increased by ~20% (see the dotted curve in the inset of Fig. 5), possibly due to ion-ion nuclear-elastic scattering [41]. This postulation, if correct, would have an impact on our understanding of DT-alpha heating of the fuel ions in an ignition experiment. Another possibility that must also be considered in explaining this discrepancy is that coupled modes of the plasma ions are not considered in these theories. However, this is unlikely, as the ion-ion coupling is weak.

In summary, ion stopping around the Bragg peak has been measured in well-characterized HED-plasma conditions. This effort significantly advances previous efforts by providing the first accurate experimental validation of ion-stopping formalisms in the regime ranging from low-velocity ion stopping—through the Bragg peak—to high-velocity ion stopping. The data indicate that the BPS formalism provides a better description of the ion stopping than other formalisms around the Bragg peak, except for the ion stopping at

$v_i \sim 0.3 v_{\mathrm{th}}$, where the BPS prediction significantly underpredicts the observation. Experimental concerns have been ruled out as an explanation of this observation. To explain the data, it is postulated that the contribution from the ion-ion component to the total ion stopping might be significantly larger than predicted by the theories, as none of them treat both ion-ion nuclear-elastic and Coulomb scattering. A 20% increase in the total ion stopping, possibly due to ion-ion nuclear-elastic scattering, is required to explain the data, which would have an impact on our understanding of the DT-alpha energy deposition and heating of the fuel ions and would thus reduce the ignition threshold in an ignition experiment. In addition, these results indicate that the unification of the relevant physics into one theory, especially around the Bragg peak, remains challenging and an unresolved problem, even for these HED-plasma conditions. They also represent a significant advance towards providing a better understanding of DT-alpha energy deposition and heating in hot-spot ignition experiments at the NIF.

The work described herein was performed in part at the LLE National Laser User's Facility (Grant No. DE-NA0003539), and it was supported in part by the U.S. DOE (Grant No. DE-NA0002949) and the Laboratory for Laser Energetics (LLE) (subcontract Grant No. 416107-G). In addition, R. F. was supported by Grant No. ENE2015-67581-R (MINECO/FEDER-UE) from the Spanish Ministry of Economy and Competitiveness.

[1] O. H. Hurricane *et al.*, Inertially confined fusion plasmas dominated by alpha-particle self-heating, Nat. Phys. **12**, 800 (2016).
[2] G. H. Miller, E. I. Moses, and C. R. Wuest, The National Ignition Facility: Enabling fusion ignition for the 21st century, Nucl. Fusion **44**, S228 (2004).
[3] M. Temporal, B. Canaud, W. Cayzac, R. Ramis, and R. L. Singleton Jr., Effects of alpha stopping power modelling on the ignition threshold in a directly-driven inertial confinement fusion capsule, Eur. Phys. J. D **71**, 132 (2017).
[4] T. A. Mehlhorn, A finite material temperature model for ion energy deposition in ion driven inertial confinement fusion targets, J. Appl. Phys. **52**, 6522 (1981).
[5] T. Peter and J. Meyer-ter-Vehn, Energy loss of heavy ions in dense plasma. I. Linear and nonlinear Vlasov theory for the stopping power, Phys. Rev. A **43**, 1998 (1991).
[6] L. S. Brown, D. L. Preston, and R. L. Singleton, Jr, Charged particle motion in a highly ionized plasma, Phys. Rep. **410**, 237 (2005).
[7] C. K. Li and R. D. Petrasso, Charged-Particle Stopping Powers in Inertial Confinement Fusion Plasmas, Phys. Rev. Lett. **70**, 3059 (1993); Charged-Particle Stopping Powers in Inertial Confinement Fusion Plasmas [Phys. Rev. Lett. **70**, 3059(E) (1993)]; **114**, 199901(E) (2015).
[8] D. Gericke, M. Schlanges, and W. Kraeft, Stopping power of a quantum plasma—T-matrix approximation and dynamical screening, Phys. Lett. A **222**, 241 (1996).
[9] G. Zwicknagel, C. Toepffer, and P.-G. Reinhard, Stopping of heavy ions in plasmas at strong coupling, Phys. Rep. **309**, 117 (1999).
[10] G. Maynard and C. Deutsch, Energy loss and straggling of ions with any velocity in dense plasmas at any temperature, Phys. Rev. A **26**, 665 (1982).
[11] G. Maynard, and C. Deutsch, Born random phase approximation for ion stopping in an arbitrarily degenerate electron fluid, J. Phys. (Paris) **46**, 1113 (1985).
[12] P. E. Grabowski, M. P. Surh, D. F. Richards, F. R. Graziani, and M. S. Murillo, Molecular Dynamics Simulations of Classical Stopping Power, Phys. Rev. Lett. **111**, 215002 (2013).
[13] D. O. Gericke, M. Schlanges, and W. D. Kraeft, T-matrix approximation of the stopping power, Laser Part. Beams **15**, 523 (1997).
[14] T. Kihara, and O. Aono, Unified theory of relaxations in plasmas, I. Basic theorem, J. Phys. Soc. Jpn. **18**, 837 (1963).
[15] The ion-ion stopping-power component is larger than the ion-electron stopping-power component for ion velocities of $v_i < 0.1 v_{\mathrm{th}}$.
[16] E. A. Frieman, and D. L. Book, Convergent classical kinetic equation for a plasma, Phys. Fluids **6**, 1700 (1963).
[17] F. C. Young, D. Mosher, S. J. Stephanakis, S. A. Goldstein, and T. A. Mehlhorn, Measurements of Enhanced Stopping of 1-MeV Deuterons in Target-Ablation Plasmas, Phys. Rev. Lett. **49**, 549 (1982).
[18] D. H. H. Hoffmann, K. Weyrich, H. Wahl, D. Gardés, R. Bimbot, and C. Fleurier, Energy loss of heavy ions in a plasma target, Phys. Rev. A **42**, 2313 (1990).
[19] G. Belyaev, M. Basko, A. Cherkasov, A. Golubev, A. Fertman, I. Roudskoy, S. Savin, B. Sharkov, V. Turtikov, A. Arzumanov, A. Borisenko, I. Gorlachev, S. Lysukhin, D. H. H. Hoffmann, and A. Tauschwitz, Measurement of the Coulomb energy loss by fast protons in a plasma target, Phys. Rev. E **53**, 2701 (1996).
[20] C. Stöckl, M. Roth, W. Süß, H. Wetzler, W. Seelig, M. Kulish, P. Spiller, J. Jacoby and D. H. H. Hoffmann, Experiments on the interaction of heavy-ion beams with dense plasmas, Fusion Technol. **31**, 169 (1997).
[21] C. Stöckl *et al.*, Experiments on the interaction of heavy ions with dense plasma at GSI-Darmstadt, Nucl. Instrum. Methods Phys. Res., Sect. A **415**, 558 (1998).
[22] M. Roth, C. Stöckl, W. Süß, O. Iwase, D. O. Gericke, R. Bock, D. H. H. Hoffmann, M. Geissel, and W. Seelig, Energy loss of heavy ions in laser-produced plasmas, Europhys. Lett. **50**, 28 (2000).
[23] A. Golubev *et al.*, Experimental investigation of the effective charge state of ions in beam–plasma interaction, Nucl. Instrum. Methods Phys. Res., Sect. A **464**, 247 (2001).
[24] K. Shibata, A. Sakumi, R. Sato, K. Tsubuku, J. Hasegawa, M. Ogawa, and Y. Oguri, A TOF system to measure the energy loss of low energy ions in a hot dense plasma, Nucl. Instrum. Methods Phys. Res., Sect. B **161**, 106 (2000).
[25] A. B. Zylstra, J. A. Frenje, P. E. Grabowski, C. K. Li, G. W. Collins, P. Fitzsimmons, S. Glenzer, F. Graziani, S. B. Hansen, S. X. Hu, M. Gatu Johnson, P. Keiter, H. Reynolds, J. R. Rygg, F. H. Séguin, and R. D. Petrasso, Measurement of Charged-Particle Stopping in Warm Dense Plasma, Phys. Rev. Lett. **114**, 215002 (2015).

[26] F. R. Graziani *et al.*, Large-scale molecular dynamics simulations of dense plasmas: The Cimarron project, High Energy Density Phys. **8**, 105 (2012).

[27] J. Jacoby, D. H. H. Hoffmann, W. Laux, R. W. Müller, H. Wahl, K. Weyrich, E. Boggasch, B. Heimrich, C. Stöckl, H. Wetzler, and S. Miyamoto, Stopping of Heavy Ions in a Hydrogen Plasma, Phys. Rev. Lett. **74**, 1550 (1995).

[28] D. G. Hicks *et al.*, Charged-particle acceleration and energy loss in laser-produced plasmas, Phys. Plasmas **7**, 5106 (2000).

[29] J. A. Frenje, P. E. Grabowski, C. K. Li, F. H. Séguin, A. B. Zylstra, M. Gatu Johnson, R. D. Petrasso, V. Y. Glebov, and T. C. Sangster, Measurements of Ion Stopping Around the Bragg Peak in High-Energy-Density Plasmas, Phys. Rev. Lett. **115**, 205001 (2015).

[30] W. Cayzak *et al.*, Experimental discrimination of ion stopping models near the Bragg peak in highly ionized matter, Nat. Commun. **8**, 15693 (2017).

[31] T. R. Boehly *et al.*, Initial performance results of the OMEGA laser system, Opt. Commun. **133**, 495 (1997).

[32] T. Nagayama, R. C. Mancini, R. Florido, D. Mayes, R. Tommasini, J. A. Koch, J. A. Delettrez, S. P. Regan, and V. A. Smalyuk, Direct asymmetry measurement of temperature and density spatial distributions in inertial confinement fusion plasmas from pinhole space-resolved spectra, Phys. Plasmas **21**, 050702 (2014).

[33] H. Sio *et al.*, A Particle X-ray Temporal Diagnostic (PXTD) for studies of kinetic, multi-ion effects, and ion-electron equilibration rates in Inertial Confinement Fusion plasmas at OMEGA (invited), Rev. Sci. Instrum. **87**, 11D701 (2016).

[34] V. Yu Glebov, C. Stoeckl, T. C. Sangster, S. Roberts, G. J. Schmid, R. A. Lerche, and M. J. Moran, Prototypes of National Ignition Facility neutron time-of-flight detectors tested on OMEGA, Rev. Sci. Instrum. **75**, 3559 (2004).

[35] C. Stoeckl, V. Yu. Glebov, D. D. Meyerhofer, W. Seka, B. Yaakobi, R. P. J. Town, and J. D. Zuegel, Hard x-ray detectors for OMEGA and NIF, Rev. Sci. Instrum. **72**, 1197 (2001).

[36] J. T. Larsen, and S. M. Lane, HYADES—A plasma hydrodynamics code for dense plasma studies, J. Quant. Spectrosc. Radiat. Transfer **51**, 179 (1994).

[37] See Supplemental Material at http://link.aps.org/supplemental/10.1103/PhysRevLett.122.015002 for the supplemental material that explicitly discusses key points of the experimental procedure and associated uncertainties.

[38] F. H. Séguin *et al.*, Spectrometry of charged particles from inertial-confinement-fusion plasmas, Rev. Sci. Instrum. **74**, 975 (2003).

[39] F. H. Séguin *et al.*, D^3He-proton emission imaging for inertial-confinement-fusion experiments (invited), Rev. Sci. Instrum. **75**, 3520 (2004).

[40] B. Tashev, F. Baimbetov, C. Deutsch, and P. Fromy, Low velocity ion stopping in binary ionic mixtures, Phys. Plasmas **15**, 102701 (2008).

[41] The differential cross sections for t-d, t-^{3}He, and t-^{40}Ar nuclear elastic scattering at relevant center-of-mass energies are poorly known and cannot be used to quantitatively assess their impact on the ion-ion stopping component.